Journal of The
Electrochemical Society

Effects of Main Aging Mechanism and State of Charge on the Safety of 21700 Li-Ion Battery Cells with Ni-Rich NMC Cathode

Journal of The Electrochemical Society, 2024 **171** 110524

Effects of Main Aging Mechanism and State of Charge on the Safety of 21700 Li-Ion Battery Cells with Ni-Rich NMC Cathode

Max Feinauer,[1] Abdelaziz A. Abd-El-Latif,[1] Peter Sichler,[1] Margret Wohlfahrt-Mehrens,[1,2] Markus Hölzle,[1] and Thomas Waldmann[1,2,3,z]

[1]*Zentrum für Sonnenenergie- und Wasserstoff-Forschung Baden-Württemberg (ZSW), Lise-Meitner-Straße 24, 89081 Ulm, Germany*
[2]*Helmholtz Institute Ulm for Electrochemical Energy Storage (HIU), Helmholtzstraße 11, 89081 Ulm, Germany*
[3]*Institute of Surface Chemistry and Catalysis, Ulm University, Albert-Einstein-Allee 47, 89081 Ulm, Germany*

It is known that both the material used in Li-ion battery cells, as well as their aging history and state of charge (SOC), strongly impact the safety of such cells. This study investigates the safety characteristics of new or aged 21700 cells containing silicon-graphite blend anodes together with Ni-rich NMC cathodes by accelerating rate calorimetry (ARC) at different SOC. Cells underwent cyclic aging at 0 °C, room temperature, or 50 °C to induce different aging mechanisms including Li plating and solid electrolyte interphase growth. The quasi-adiabatic heat-wait-seek ARC tests show lower temperatures for self-heating (SH), CID triggering, venting, and thermal runaway (TR) with increasing SOC, indicating reduced safety levels. Furthermore, the mass loss and TR intensity increase as the SOC of the cell increases. Aged cells show a similar SOC dependence as new cells in view of venting and TR, although both temperatures are reduced. The onset of SH at around 35 °C, independent of SOC, reveals a significant safety issue in cells with Li plating. Additional cell voltage monitoring and on-line mass spectrometry provide further insights into the decomposition processes. Our findings provide essential knowledge to improve the safety and design of Li-ion battery cells by identifying unsafe states.

 [DOI: 10.1149/1945-7111/ad9356]

Manuscript submitted May 26, 2024; revised manuscript received October 25, 2024. Published November 27, 2024.

Supplementary material for this article is available online

As Li-ion batteries become an increasingly integral part of our daily lives, understanding their safety implications becomes paramount. In order to ensure the reliable and safe operation of Li-ion batteries over their lifetime, it is essential to comprehensively understand the various parameters that affect safety. High energy containing batteries require a careful handling because their battery materials typically have lower intrinsic safety characteristics.

The need for higher specific energy and energy densities in batteries can be realized by replacing increasing proportions of the graphite with silicon in the anode.[1] On the cathode side, the energy density is increased by increasing the amount of Ni in the NMC ($LiNi_xMn_yCo_{1-x-y}O_2$) material.[2,3] However, Ni-rich NMC materials are also known to have a reduced thermal stability due to high Ni-content, which directly correlates with increased oxygen release at rather low temperatures.[2–6] The amount of Mn in the NMC material dominates the thermal stability and increases cycle life, but at the same time reduces energy density.[2,3] LFP ($LiFePO_4$) as an alternative cathode material has a superior thermal stability compared to NMC or NCA ($LiNi_xCo_yAl_{1-x-y}O_2$), but has at the same time a much lower energy density.[7–9] Today, NCM with a Ni-content of $x > 0.85$ is the dominating cathode material in high-energy battery cells.

In view of cell safety, it is expected that cells with high energy content also show a more pronounced thermal runaway (TR) reaction.[10] Ultimately, any TR is triggered by an increase in temperature, as mechanical or electrical defects typically lead to local heat generation, which triggers further reactions.[11] Once the heating rate exceeds the heat dissipation rate, cells will self-heat and in the worst case might experience a TR.

There is a wide variety of safety testing methods and abuse cases to trigger a TR. However, the safety testing method can have a significant impact on the result and could even be different for new and aged cells.[12,13] Accelerating rate calorimetry (ARC) is a valuable and well-established safety testing method for investigating the case of a perfectly insulated battery under quasi-adiabatic conditions.[14–18] In particular heat-wait-seek (HWS) tests in ARC experiments are used to determine safety critical temperatures such as the onset of self-heating (SH), venting, or TR.

The onset of SH is linked to the decomposition of the metastable solid electrolyte interphase (SEI), followed by an exothermic reduction of the electrolyte, leading to the formation of a more inorganic SEI.[19,20] The SEI reformation process is directly influenced by the lithiation degree of the anode, i.e. the state of charge (SOC) of the cell, resulting in an increasing onset temperature of SH (T_{SH}) with decreasing SOC.[4,8,9,21,22] This SEI reformation process coincides with anode decomposition.[19,20] The anode decomposition has a higher onset temperature, generates more heat, and shows no SOC dependence.[19,20]

Once the SH of the battery has started, a series of safety devices come into play to reduce the risk of uncontrolled TR. In cylindrical cells, these include usually the current interrupt device (CID), which is designed to electrically disconnect the cell, and venting mechanisms, which relieve internal gas pressure in a controlled way to prevent case rupture.[23] Additionally, a positive temperature coefficient (PTC) resistor and shutdown separators can be incorporated to interrupt the current flow, if the cell temperature becomes too high.[23]

However, due to the large energy content in a Li-ion battery, high-energy TR reactions might occur, resulting in a large amount of heat and gas being released and, in the worst case, also fire and explosion.[24] In general, the reaction that causes this accelerated heat generation depends not only on the chemistry of the battery materials, but also on the SOC of the cell. At high SOC, the cathode is in a more de-lithiated state and, in particular, the NMC structure is very unstable.[20] This results in a decrease in the decomposition temperature and an increase in the amount of oxygen released during such decomposition. This released oxygen leads to electrolyte decomposition or better to say electrolyte burning.[20] As observed in many experiments, a high SOC correlates with a low TR onset temperature and the TR intensity could vary by three orders of magnitude.[8,9,19,25–31] Zhao et al. found a further correlation between a low TR onset temperature and a high maximum temperature for cells at high SOC.[32] Barkholtz et al. did not observe any

[z]E-mail: thomas.waldmann@zsw-bw.de

decomposition of the layered lithium metal oxide under oxygen release at 0% SOC.[19]

As batteries age, the ongoing processes towards the TR of the battery may change, particularly as a function of the underlying degradation mechanisms. The initial SEI layer changes from an organic to a thicker and more stable inorganic layer during aging, i.e. the energy content in the fully charged state decreases during aging without forming a more reactive species.[15,17,22,27,33–35] Thus, aging with SEI growth, either due to calendar or cyclic aging, results in an increased onset of SH temperature.[22,27,34,35] In contrast to that, aging with Li plating as the dominant aging mechanism can reduce the safety properties, because the plated Li reacts violently with electrolyte even at very low temperatures.[12,14–17,20,22,26,35–37] In aged cells with Li plating, the energy content in the fully charged state is indeed decreased but at the same time a more reactive species is formed. Li plating is the result of high anode polarization during charging at low temperatures or fast charging to high SOC.[38–40]

Electron impact mass spectrometry (MS) has become an indispensable tool for the detection of volatile species.[41] Coupling MS with ARC (ARC-MS) has recently been introduced by Abd-El-Latif et al.[16] to study the gases produced during the TR of new and aged Li-ion batteries. ARC-MS can provide valuable insights into the evolution of hazardous gases during cell venting or TR, i.e., exothermic chemical reactions and thermal decomposition processes.[16,17] ARC-MS can also be combined with other sensors and allows for a more comprehensive understanding of the degradation stages of battery cells and enhances the ability to characterize and understand complex chemical reactions and thermal processes.[16,17]

Previous research has predominantly examined either the impact of SOC[7–9,19,25–31,42] or the effect of aging[12,15,17,22,32,35,37,43–45] on the safety of Li-ion cells. The aim of this study is to investigate the combined effect of SOC *and* aging on safety of state-of-the-art Li-ion cells. This investigation is crucial for gaining a comprehensive understanding of various factors influencing the thermal stability of battery cells. This study evaluates one cell-type across various SOC levels and aging mechanisms to detect any shifts in thermal behavior and monitor the evolved hazardous gases. The ARC-MS method was used to analyze 48 commercial cylindrical 21700 Li-ion cells with different aging history. The cells were cyclically aged at temperatures of 0 °C, room temperature (RT), or 50 °C to induce different degradation mechanisms, including Li plating and accelerated SEI growth. The aging of the cells was stopped when the cells have reached a state of health (SOH) of 80%. Differential voltage analysis (DVA) is further applied to the new and aged cells to identify the degradation mechanism.

Experimental

21700 cell characterization.—Commercially available cylindrical 21700 Li-ion cells with a nominal capacity of 4.85 Ah (17.6 Wh) and a voltage range from 2.5 V to 4.2 V were used for his study. The average cell impedance at 1 kHz was determined to be (22.7 ± 0.2) mΩ using a Hioki BT 3554 battery.

Post-mortem analyses had been delivering additional information. By using a JEOL IT-500 scanning electron microscope (SEM), a spherically shaped layered oxide was found as cathode materials and potato shaped graphite particles as anode active material. Energy dispersive X-ray spectroscopy (EDX) measurements confirmed a Ni-rich NMC blended with approximately 4% of pure $LiNiO_2$. Inductively coupled plasma optical emission spectroscopy (ICP-OES) of the cathode active material using a Spectro Arcos SOP system confirms the Ni-rich NMC with a $LiNi_{0.834}Mn_{0.059}Co_{0.107}O_2$ stoichiometry, including the $LiNiO_2$. EDX measurements of the anode showed a Si-graphite composite electrode with ∼1.85 wt% Si.

Scanning thermal analysis (STA) which is a combination of differential scanning calorimetry (DSC) and thermal gravimetric analysis (TGA) was performed on the separator using a STA 449 C device from Netzsch. An endothermic peak in the range of 120 °C to 140 °C is typical for a polyethylene (PE) separator. Additional SEM-EDX analysis of the separator showed a ceramic coating (Al_2O_3) facing the cathode side.

Table I. Overview of the number of cells tested at a certain SOC for new and aged cells.

SOC/%	New	0 °C aged	RT aged	50 °C aged
100	5	3	3	3
80	2			
70	3	2	2	
50	4	2	2	2
30	3	2	2	
10	3	2	2	
0	1			

Cyclic aging and SOC setting.—The cyclic aging of the battery cells was conducted with a BaSyTec CTS. The cells were charged to the upper cut-off voltage of 4.2 V with a constant current (CC) of 0.5 C, followed by constant voltage (CV) charging with a cut-off current of 0.05 C. Discharging was performed in the CC mode with 0.5 C until the lower cut-off voltage of 2.5 V was reached. A check-up cycle with 0.1 C charge/discharge was performed every 50 cycles. This check-up cycle was further used for DVA.

All cells had been aged by cycling as indicated above: eleven cells at RT (∼25 °C), additional eleven cells at 0 °C and five cells at 50 °C in Vötsch climate chambers with active air circulation. While charging and discharging at 25 °C with 0.5 C is fully within the specified operating window, charging with 0.5 C at both 0 °C and 50 °C slightly overshoots the operating window specified by the manufacturer. A holding time of 10 min is used after each charging and discharging step to allow the battery cells to cool down as they significantly heat up during cycling.

The cyclic aging was repeated until the capacity drops below (80 ± 2)% of its initial capacity at the given temperatures. The capacity of the last discharge step was used to calculate both the final SOH and to define the SOC. Therefore, the cells were fully discharged with 0.5 C to the lower cut-off voltage and subsequently charged with 0.5 C in the CC or CC-CV mode until the desired SOC was reached. Full charge (100% SOC) was defined by a current falling below a rate of 0.05 C in the constant current phase. Charging was done at the aging temperature to ensure no change in the aging mechanism, which in particular could affect cells with Li plating if charged or stored at elevated temperatures.[14] An overview of all tested cells is given in Table I.

Three 0.5 C charge/discharge cycles were conducted with the new battery cells at RT prior to the final charge to the desired SOC for the ARC test. The nominal capacity was used to set the SOC of the 21 new cells. After charging the cells, the ARC tests were started within less than an hour.

Accelerating rate calorimetry.—An ARC-ES device from Thermal Hazard Technology (THT, UK) was used to provide quasi-adiabatic conditions to the cell under investigation and to step-by-step increase the cell temperature until T_{SH}. A Hioki battery tester (BT 3560) was used to track the cell voltage and impedance at 1 kHz during the ARC test.

The cells were prepared for the ARC tests by removing the shrink foil and by crimping the wires for voltage and impedance measurement to the outer cell terminals. An exception to the removal of the shrink foil was made for a separate test to investigate the effect of the shrink foil on the overall thermal

propagation process. Polyamide tape was used to provide electrical insulation around the positive tab. The cell, together with the sample thermocouple (N-type), was then fixed in a thin steel holder to allow the cell to hang freely from the top of the ARC reaction vessel. A calibration and subsequent drift check of the ARC system with an empty 21700 size can ensured the correct heating power of the heaters in the ARC device to provide quasi adiabatic conditions.

A heat-wait-seek (HWS) program was applied during the ARC experiment to study the critical temperatures of the 21700 cells. Starting from 35 °C, the temperature was gradually increased in steps of 5 K with a heating rate in the range of 0.1 K min^{-1}, followed by a 15 min waiting period to allow a homogeneous temperature distribution. During the subsequent 10 min seek period, the temperature changes were tracked. When the resulting self-heating rate (SHR) rose above the exothermic sensitivity of 0.02 K min^{-1}, the cell reaction was defined as exothermic and no further heating steps of the ARC were conducted. At T_{SH}, where the exothermic sensitivity is exceeded for the first time, the onset of SH is reached. This temperature can be considered as the first safety relevant characteristic temperature in an ARC test.

Coupling of ARC with mass spectrometry.—The previously developed combination of ARC and MS via a gas inlet probe and Swagelok valve is described in detail by Abd-El-Latif et al.[16] For the qualitative and semi-quantitative study of the gases released during TR, the MS (HPR40, HIDEN Analytical, UK) was connected to the ARC device via a gas inlet probe and a Swagelok valve. An extra Teflon membrane (PF-002H, Hangzhou Cobetter Filtration Equipment Co., LTD, China) was fitted to the gas inlet probe to prevent the diffusion of dust and electrolyte into the vacuum system of the MS.

Prior to the ARC-MS experiment, the Swagelok valve was gently opened until the vacuum reached 10^{-6} mbar. Several ionic signals of the expected fragments were recorded simultaneously during the thermal abuse test such as hydrogen ($m/z = 2$), CO_2 ($m/z = 22$ and 44), ethylene ($m/z = 26$, 27, and 28), oxygen ($m/z = 32$), argon ($m/z = 40$), POF_3 ($m/z = 85$ and 104), and organic solvents e.g. EMC (I_{45}, I_{59} and I_{90}, which have a relative intensity of 0.65, 0.2, and 0.1 of the main peak at $m/z = 29$, respectively) and DMC (I_{45} is the main peak and $I_{59} = 0.75\ I_{45}$). The background of the $m/z = 40$ signal was used as an indicator of the efficiency of the ion source. The results presented have been normalized to the baseline of the corresponding signal in order to exclude filament life time effects of the MS.

Effect of shrink foil in ARC HWS testing.—To investigate the effect of the shrink foil on the thermal hazard characteristics and the evolved gases during the TR of the cells, ARC-MS HWS measurements were performed on two cells each with and without shrink foil under the same experimental conditions. New 21700 cells at 100% SOC were selected for this comparison.

The DSC analysis (see Fig. S1) of the shrink foil material shows characteristic endothermic peaks at 77 °C, 250 °C, and 408 °C and an exothermic peak at 120 °C. These are attributed to the characteristic glass transition, melting, decomposition, and recrystallization temperatures of the shrink foil material, respectively. The TGA curve (see Fig. S1) shows that the weight of the sample is stable up to 350 °C, where it sharply drops to 22% of the initial mass. Based on the database of thermoplastic materials, these features can be assigned to polyethylene terephthalate (PET) polymer.

The characteristic temperatures determined in the ARC test showed no significant effect of the shrink foil, as can be seen in Fig. S2. As the HWS test in ARC is usually very slow, any potential increase in temperature difference due to the shrink foil between the cell core and the cell surface, where the temperature measurement takes place, appears to be negligible.

The MS signals (Fig. S3) show that the detection of any expected volatile species is independent of the presence of the shrink foil, as the thermal decomposition of this shrink foil takes place above 400 °C, well above the thermal abuse parameters of the new 100% SOC cell. For all subsequent ARC HWS tests, the cells were measured without the PET shrink foil.

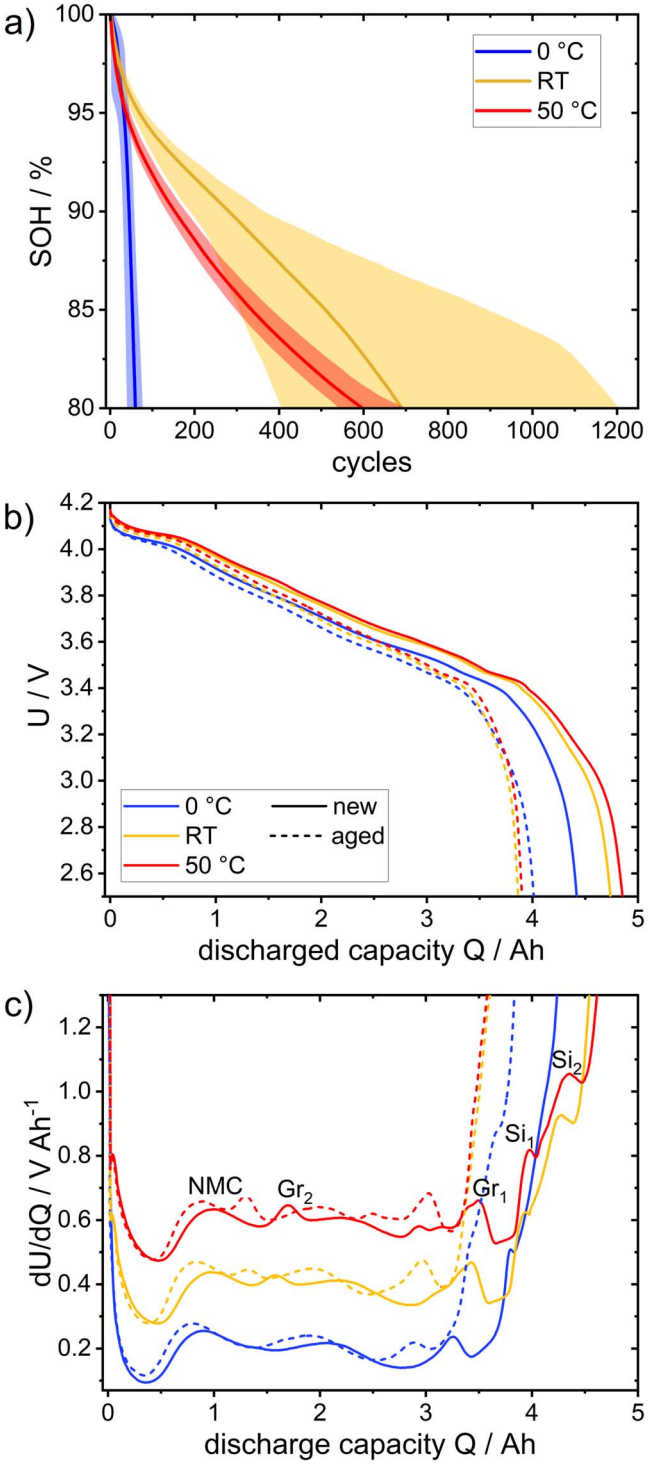

Figure 1. (a) Cyclic aging curves of 21700 cells aged at different temperatures. Solid lines give the average aging curve while the shading marks the region between the slowest and fastest aging curve. (b) Discharge voltage curves of new (solid line, 100% SOH) and aged cells (dashed line, ~80% SOH) for the three different aging temperatures. (b) DVA curves derived from the voltage curves shown in (b). The curves for RT and 50 °C cells have been vertically shifted by 0.2 V Ah^{-1} and 0.4 V Ah^{-1}, respectively. Material distinctive DVA peaks for Si, graphite (Gr), and NMC are exemplarily marked for the new 50 °C cell.

Results and Discussion

Temperature dependent aging behavior.—Cyclic aging of the 21700 cells was performed at different temperatures, triggering different aging mechanisms. The averaged aging curves and the range between the slowest and fastest aging curves are shown in Fig. 1a. The average aging curve was calculated by averaging the number of cycles for each SOH. By searching for the minimum and maximum number of cycles for each SOH, the fastest and slowest aging curves are found for all cells tested.

While the aging curves for all cells at 0 °C and 50 °C are in a narrow range, aging at RT varies significantly. The average number of cycles to 80% SOH with corresponding standard deviation is 60 ± 13 cycles at 0 °C and 600 ± 60 cycles at 50 °C. The rapid capacity degradation at 0 °C and the fact that the capacity fade at this temperature is increased compared to RT clearly indicates Li plating as the dominant aging mechanism.[17,39,46,47] In contrast, aging at 50 °C is also faster than at RT and is most likely driven by accelerated SEI growth, showing a typical temperature dependent aging behavior.[17,39,46,47] At RT, an average number of cycles of 690 ± 280 is achieved. The number varies by a factor of three from 400 to 1,200 cycles, even if all cells are cycled at the same time under the same conditions. However, the extent of such extensive scattering is atypical for commercial cells. Especially since the standard deviation of the initial capacity and the internal resistance of the cells is less than 1%.

For a similar cell type, we found that at 25 °C, i.e. close to RT, the transition of the temperature dependent dominant aging mechanism from Li plating at low temperatures to SEI growth a high temperature occurs.[46,48] Thus, even small variations in the aging temperature might already trigger Li deposition as a more severe and therefore dominant aging mechanism, which could explain the large variations in the aging curves.

For all cells, the resistance, as measured by the IR drop at the start of discharge, increased approximately linearly from the beginning of life to the end of life by approximately 10 mΩ or 25%. This direct relationship between resistance increase and capacity fade confirms previous findings.[11,49,50]

The discharge voltage curves for the new cells (solid lines) and cells aged to ∼80% SOH (dashed lines) at three different temperatures are shown in Fig. 1b. The first and last 0.1 C check-up cycle during cyclic aging at 0 °C, RT, or 50 °C is plotted. For each aging temperature, a representative cell was selected that was closest to the average aging curve in Fig. 1a. Further analysis of the aging process is carried out using DVA of these discharge curves. The DVA curves for new and aged cells are shown in Fig. 1b. The material characteristic peaks for the NMC cathode and the Si-graphite composite anode are marked according to Zilberman et al.[51]

For the cells aged at RT or 50 °C it can be seen that both characteristic peaks for Si (Si_1 and Si_2) disappear and the slope of the curve increases at the end of discharge. This indicates loss of anode active material (LAAM), particularly as the distance between the first pure graphite peak (Gr_1) and the end of discharge capacity decreases, which includes the storage capability of Si. LAAM is a typical contributor to the degradation of Si-based Li-ion battery cells. The increased volume change during cycling leads to particle cracking with loss of electrical contact and rapid growth of resistive surface layers blocking active sites and consuming active Si.[1,51,52]

Comparing the distance between the graphite peaks Gr_1 and Gr_2 gives an indication of the storage capability of the graphite component.[51] As the shift of both peaks to the right is similar, a small contribution of graphite to LAAM during RT or 50 °C aging can be concluded. LAAM in case of graphite might, for example, originate from contact loss of graphite particles in the anode.[53]

For aging at 0 °C, only the S_1 peak from the two Si characteristic peaks is weakly visible, indicating a lower contribution of the Si component to the total capacity at lower temperatures. The S_1 peak does not completely disappear in the aged state at 0 °C, implying a smaller contribution of LAAM to the total capacity loss due to partial loss of the Si component in the anode.

Further consideration of the marked NMC peak could provide information on loss of Li inventory (LLI) by comparing the cathode with the central graphite anode peak (Gr_2).[54] However, as the Gr_2 peak has been further shifted by LAAM, it is not possible to clearly attribute the decreasing distance between these Gr_2 and NMC peaks during RT and 50 °C aging to LLI.[51] As the prominent Gr_2 peak is not visible at 0 °C, it is also not possible to differentiate between LAAM and LLI. Finally, as suggested by Zilberman et al., the distance between the NMC peak and the valley immediately to the right, can provide information on the NMC storage capability.[51] As can be seen in Fig. 1c, this distance decreases for all aging temperatures, indicating loss of cathode active material (LCAM).

In conclusion, the capacity degradation at RT and 50 °C is driven by LAAM of the Si component, with additional contributions from LLI. The Li is most likely lost in electrically isolated particles or consumed by side reactions such as SEI growth on graphite and the Si component, which dominates the degradation at high temperatures. One difference here is that SEI growth on graphite does not consume graphite (no contribution to LAAM), however, SEI growth on the Si component consumes Si (contribution to LAAM). These findings are consistent with the results reported by Flügel et al.[1] Due to the limited distinctive peaks at 0 °C, it is not possible to distinguish between the individual degradation mechanisms at this temperature. However, the fast capacity fading in particular gives evidence for Li plating as the dominant aging mechanism with significant LLI, since Li is irreversibly lost due to SEI growth on the Li surface and in form of electrically disconnected "dead Li."

SOC dependent thermal runaway process.—The SHR, particularly as a function of temperature, provides information on the exothermic reactions taking place within a cell. Many thermal parameters and characteristic temperatures can be determined by logarithmically plotting the SHR vs temperature. Such plots are shown in Fig. 2 for new, 50 °C aged, RT aged, and 0 °C aged cells at different SOC.

The onset of SH, i.e. when the SHR exceeds the exothermic sensitivity of 0.02 K min^{-1}, corresponds to the first data point in the SHR vs temperature plot. At the beginning of the SH of a cell, the protective SEI layer of the anode breaks down causing exothermic reactions due to the reaction between the electrolyte and the intercalated Li.[20] The reformation of a more inorganic SEI continues as long as there is enough Li intercalated in the anode, i.e. in particular at low SOC the damaged SEI layer could only be repaired to a limited extent.[19,20,55,56] Interestingly, as can be seen in particular for the new cells in Fig. 2a, the SHR slightly decreases after the onset of SH before the almost linear increase with temperature begins. This indicates a non-negligible contribution of endothermic SEI decomposition reactions exceeding the rate of exothermic SEI reformation reactions.[34] Slightly delayed to the reformation of the more inorganic SEI, the anode degradation itself begins to overlap and produces even more heat. However, the anode degradation is independent of the SOC in contrast to the SEI decomposition and regeneration.[19,20] These ongoing exothermic reactions in the cell result in an increasing temperature, further increasing the reaction rate due to the Arrhenius law. Thus even further reactions could be triggered because the overcoming of their activation barriers becomes more probable.

As a side product of the SEI reformation, gas is formed which accumulates inside the cell can, rising the internal pressure. Once the internal pressure becomes too high, the CID is triggered pushing the burst disk outwards and thus interrupting the electrical connection between jelly roll and can. This point is determined by the sudden drop of the voltage signal as can be seen Fig. 3. As the open circuit voltage (OCV) largely varies with SOC, in Fig. 3 the difference of the measured voltage U and the initial voltage U_0 at RT is plotted.

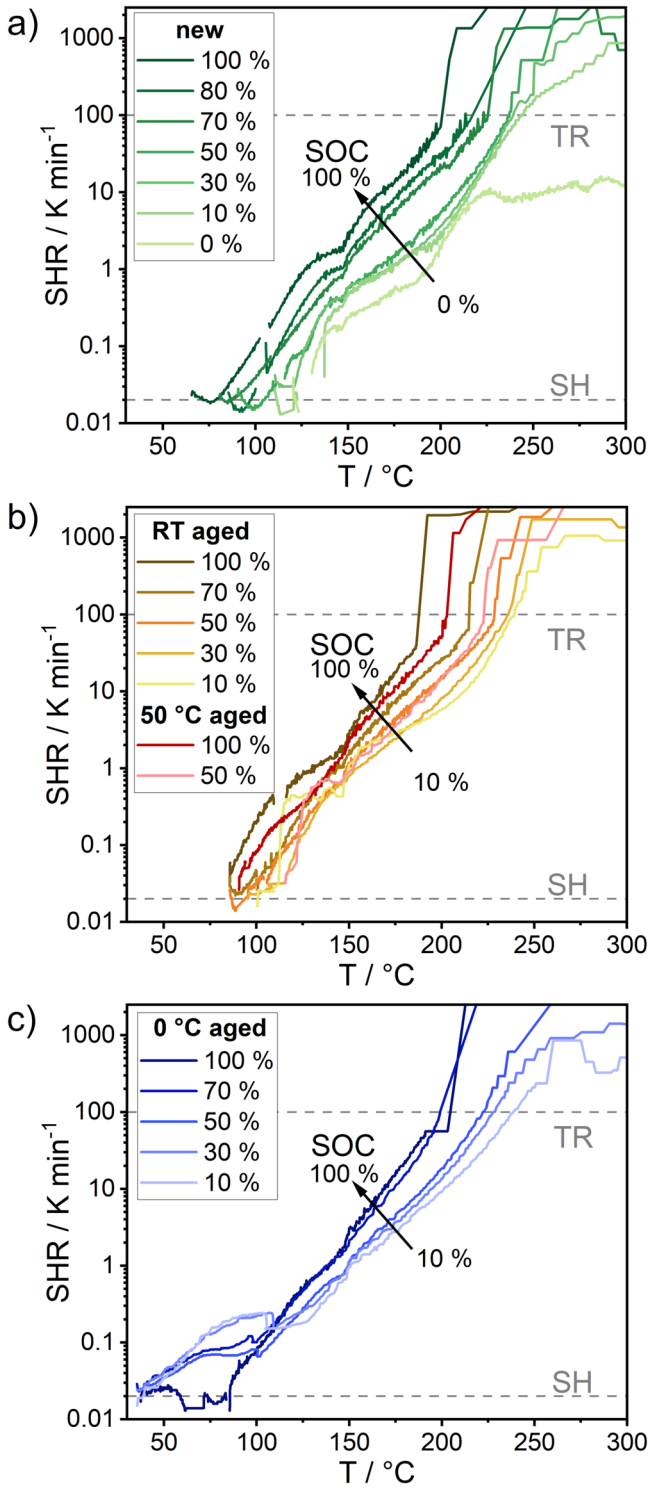

Figure 2. Self-heating rate (SHR) as function of temperature during ARC tests for different SOC and aging states: (a) new cells, (b) RT and 50 °C aged cells, and (c) 0 °C aged cells. The dashed lines mark the SHR thresholds for the onsets of SH and TR.

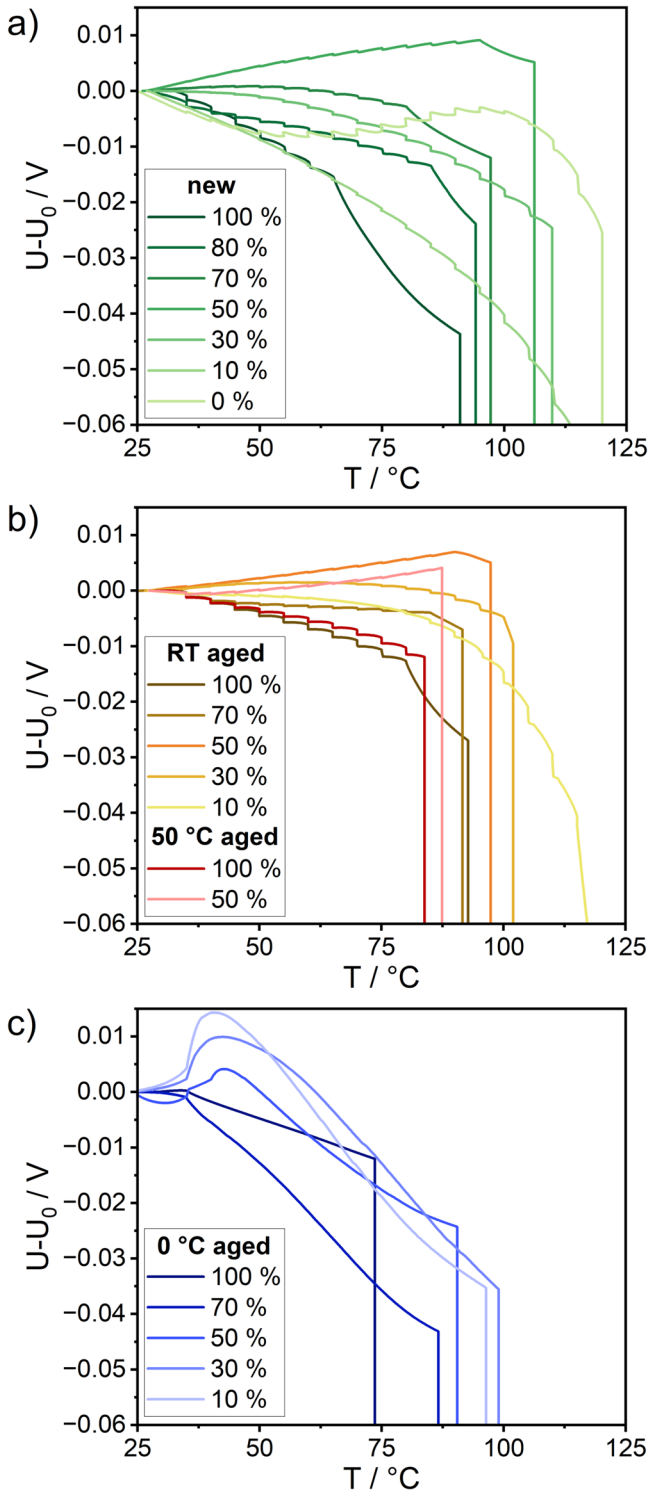

Figure 3. Cell voltage change as function of temperature during ARC tests for different SOC and aging states: (a) new cells, (b) RT and 50 °C aged cells, and (c) 0 °C aged cells. The sudden voltage drops mark the CID triggering.

Particularly in the case of ARC HWS tests without current flow, triggering the CID will not stop the decomposition reactions in the cell, however, the reactions and any possible gas formation will continue. The further increase in pressure inside the cell leads to the venting of the cell by opening the rupture disk. For different cell types investigated by others, the vent activation pressure in cylindrical cells is in the range of 1–2 MPa, which is approximately twice the CID activation pressure.[23,57] The venting temperature T_{vent} can be determined in the plot of the SHR vs temperature by the last point before the curve is interrupted at around 110 °C (see Fig. 2). The interruption results from negative SHR values due to a cooling effect of the gas streaming out during venting (Joule-Thomson effect). Note that further heating steps after the onset of SH can also cause interruptions. Temperature vs time graphs are therefore more suitable for determining the cell venting by a

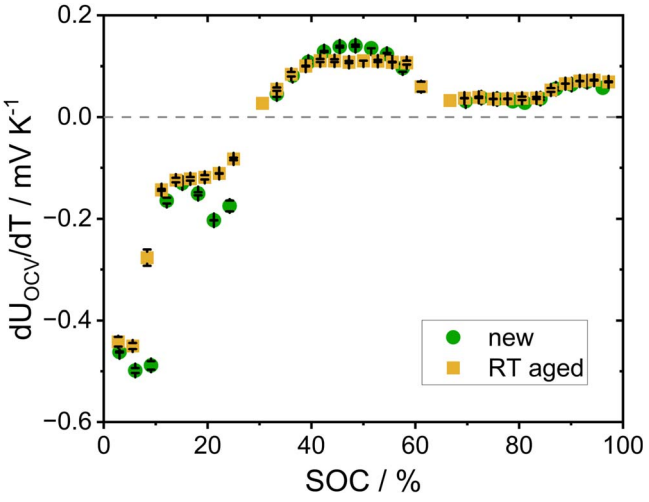

Figure 4. Temperature dependent change of the open circuit voltage of new and RT aged cells as a function of the SOC.

dip in the temperature curve (see Fig. S4). As can be seen for all the SHR curves in Fig. 2, the venting does not affect the SHR, indicating that the reactions are not relevantly influenced by the venting process and subsequent possible ambient air contact.

The SHR curves show a plateau at around 130–140 °C, indicating the endothermic melting of the separator, correlating well with the melting point of the PE separator previously determined by TGA. This plateau (see Fig. 2) in the SHR curve is generally independent of the SOC and aging state.

The rate of exothermic reactions increases as the electric energy stored increases, i.e. as the SOC increases.[10] This results in a shift of the SHR curves towards lower temperatures and thus shorter test duration with increasing SOC. This trend is observed for the new cells, as well as aged cells in Fig. 2 and is consistent with other cell types.[2,8,19,27,30,42,58]

When the SEI on the anode is fully degraded, the anode surface is no longer protected from the electrolyte and further exothermic reactions between the anode and electrolyte can occur.[9] The cell temperature begins to rise more rapidly in a self-accelerating manner due to higher rates of exothermic reactions at the anode and cathode. This is also called TR and could result in cell explosion. In literature, there is no specific definition of the onset of TR. Several groups use different techniques and threshold values to define the onset of TR.[12,14,20,28,37,59–61] A common definition, which we have applied previously, is the abrupt increase in the SHR at around 100 K min^{-1}.[16,17] T_{TR} refers in the following to the onset of TR temperature.

Figure 2 shows a similar trend of increasing reactivity with increasing SOC for both new and aged cells. This is visible on the one hand by a shift of the SHR curves towards lower temperatures with increasing SOC, which is directly correlated to lower onset temperatures of SH and TR (see next section). On the other hand, the maximum SHR at temperatures >200 °C tends to increase with increasing SOC, too. This SOC dependent TR behavior is consistent with the results of other groups.[7,8] As can be seen in Fig. 2a, the cell at 0% SOC does not produce sufficient heat to trigger a TR and, thus, 10% is chosen as the lowest SOC for the following investigations with aged cells.

Measuring the voltage is not only relevant to determine the CID triggering, it can also provide information about the ongoing decomposition processes occurring within the cell. However, the OCV of a cell is also known to be temperature dependent. Thus, the cell voltage will change during the ARC HWS tests. The ARC heating steps are therefore visible through the voltage steps in Fig. 3. The temperature dependent change of the OCV (dU_{OCV}/dT) overlaps at higher temperatures with the voltage drop resulting from Li de-intercalation to repair the damaged SEI layer. The dU_{OCV}/dT is unique for each cell type and strongly depends on SOC (see Fig. 4). However, as can be seen in Fig. 4, dU_{OCV}/dT as a function of SOC is very similar for new and RT aged cells. Details of the measurement procedure for the data in Fig. 4 are described by Feinauer et al.[62] and Plett.[63] A total of four cells with a stepwise SOC variation of 3% are used in a temperature range of 0 °C to 50 °C with 10 K steps. Nevertheless, the determination of dU_{OCV}/dT is not feasible at all SOC due to the nonlinear variation of the voltage with temperature (for instance, at ca. 0%, 30%, 60%, or 100%).

As illustrated in Fig. 4, the OCV may exhibit a decrease or increase with temperature as a function of SOC. This phenomenon is likely attributed to the entropy changes within the cell resulting among others from the staging behavior of the lithiated graphite anode. The dU_{OCV}/dT data presented in Fig. 4 provides insights into the relationship between the voltage and temperature in Fig. 3. For instance, the highest value of dU_{OCV}/dT at 50% is clearly visible in Figs. 3a and 3b, where it corresponds to the strongest increasing voltage. At SOC > 70% the dU_{OCV}/dT data suggest a slightly increasing voltage with temperature. However, the voltage curves in Fig. 3 show a decreasing voltage, which cannot be easily explained. It seems likely that additional contributions leading to a decreasing voltage are overlapping.

Moreover, at the point where the heating steps conclude in Fig. 3, namely the onset of SH, the voltage drops rapidly, regardless of its preceding behavior. The onset of SH is caused by early exothermic SEI decomposition and regeneration reactions, which result in extensive de-intercalation of Li to reform the SEI. This is evident by the decreasing voltage. However, the nonlinear shape of the cell's voltage curve (see Fig. 1b) further overlaps with the observed voltage changes in Fig. 3.

It is noteworthy that the decreasing voltage is not discernible for the cells aged at 50 °C, as the CID triggering occurs prior to the onset of SH is reached. This is attributed to a more pronounced gas evolution and a higher onset of SH. It is likely that the production of gas during the aging process at elevated temperatures has resulted in the accumulation of gas within the cell prior to the ARC test.

Effect of main aging mechanism on thermal runaway.—So far, the focus has been on general SOC dependent trends. We will now focus on the effect of cell aging at different temperatures in combination with different SOC.

While the SHR curves of new (Fig. 2a) and of RT or 50 °C aged (Fig. 2b) cells behave very similarly in the low temperature range around the onset of SH, the 0 °C aged cells differ significantly (Fig. 2c). The violent reaction of the plated Li on top of the anode with the electrolyte leads to a strong heat release even at low temperatures.[14,15,20,37,64] The 0 °C aged cells have a high amount of irreversibly plated Li that did not re-intercalate or was not stripped during the discharging step immediately after the Li plating occurred in the charging step. During cyclic aging, the amount of irreversibly plated Li accumulates to an amount that is likely much higher than the amount of reversibly plated Li within one cycle. Therefore, the amount of Li plated on the anode surface is expected to be only slightly dependent on the SOC. On the contrary, as can be seen in Fig. 2c, the SHR in the first part of the ARC HWS test up to about 110 °C increases with decreasing SOC. Interestingly, the low SHR of the 100% SOC cell at the beginning leads to much longer measurement times compared to all lower SOC. Nevertheless, the SHR was so high that the ARC device did not carry out any further heating steps. Such an SOC dependent self-heating behavior cannot be explained by parasitic reactions of Li with electrolyte. Similar experiments by Galushkin et al. did not show such an increased heating behavior for lower SOC.[26] Nevertheless, no details on rest times after cycling are known from the reported experiments. However, rest times were shown to have a significant influence on the safety behavior.[14]

As the temperature increases, the intercalation of plated Li into the electrode becomes more likely.[65] For the cells at 100% SOC, the

anode is almost fully lithiated and most of the nearest-neighbor sites are filled, resulting in an increasing overpotential which makes re-intercalation of Li less favorable (see low SHR at 100% SOC in the Fig. 2c).[64] At lower SOC, the part of the plated Li which has not yet reacted with electrolyte, can re-intercalate into graphite and alloy with the Si compound,[66–70] likely leading to the increased SHR. The evidence for Li re-intercalation is further reinforced by the voltage curves in Fig. 3c. The almost abrupt increase in cell voltage in Fig. 3c at 35 °C is due to the fact that the end of the heating steps had already been reached and the temperature rise was therefore much slower. When plotted over time, the initial increase in voltage is continuous, indicating that no temperature dependent OCV is responsible for the increase in voltage. It is more likely that a re-intercalation of the plated Li has led to this increasing voltage. Unfortunately, a quantification of the amount of re-intercalated Li appears to be difficult due to a superposition with other effects such as reaction of the plated Li with electrolyte and the decomposition and subsequent regeneration of the SEI at elevated temperatures. A similar effect of increased heating rate was found by Lian et al.[71] after charging at a high C-rate, which could imply similar re-intercalation processes and reactions with the electrolyte of the deposited Li.

In the temperature range above ∼120 °C up to TR, the SHR curves are similar for all aging states for a given SOC. A similar slope of all curves indicates a similar activation energy of the ongoing reactions. However, an exception is made here for the 0 °C aged cells, which were initially characterized by a high SHR. The reactivity of these cells is slightly reduced, as indicated by a lower slope of the SHR curves.

The behavior of the cells at TR is then again similar for cells in all aging states. However, all aged cells have lower TR onset temperatures. There is also a slight trend towards a lower maximum SHR for aged cells compared to the new cells. This may be related to the lower electrical energy content at the same SOC and the electrolyte consumption during the aging process, which reduces the heat generation from reactions, particularly between anode and electrolyte.[35]

Evaluation of characteristic temperatures.—This section can be seen as a summary of the previously discussed observations with a particular focus on the characteristic temperatures. According to the previously proposed definitions of the characteristic temperatures, the temperatures for the onset of SH (T_{SH}), CID triggering (T_{CID}), venting (T_{vent}), and onset of TR (T_{TR}) are determined for all cells at different SOC and aging states. However, the comparison of new and aged cells at the same SOC suffers from different electrical energy contents. Aged cells at 80% SOH have an approximately 20 % lower energy content. The characteristic temperatures are therefore plotted as a function of both, SOC and charged energy, in Fig. 5.

The first critical temperature on the way to the TR is the onset of SH. As can be seen in Figs. 5a and 5b, T_{SH} decreases within some scattering approximately linearly with increasing SOC for new cells and aged cells without Li plating, which is consistent with previous studies.[4,8,9,15,21,22] T_{SH} behaves similar for new and RT aged cells as a function of both SOC and charged energy in Figs. 5a and 5b.

Aging at elevated temperatures, i.e. 50 °C, results in an increase in T_{SH} of approximately 10 K. However, the 50% and 100% SOC data points in Figs. 5a and 5b show that the trend of a decreasing T_{SH} with increasing SOC is still valid. Although the onset of SH is triggered by the decomposition of the SEI, a thicker and more inorganic SEI due to high temperature aging slows down the exothermic SEI reformation process and thus increases T_{SH}.[34]

The onset of SH is drastically reduced to less than 40 °C for cells aged at 0 °C with Li plating. A low T_{SH} was also found for other cells types with Li plating with different cell chemistries.[14–16,20,26,72] In cells with Li plating, rather the reaction of Li with electrolyte than the SEI decomposition is the driving reaction for the onset of SH. In case of Li plating, no dependence on SOC or energy content was detected for the onset of SH (see Figs. 5a, 5b). This is because the exothermic reaction of the electrolyte and plated Li is mostly SOC independent. The elimination of the SOC dependence for cells with Li plating matches well with the results of Galushkin et al.[26] and Friesen et al.[20] Furthermore, more pronounced aging leads to lower T_{SH}.[17,26]

The CID trigger temperature follows a similar linearly decreasing trend with increasing SOC as T_{SH} (see Figs. 5c and 5d). T_{CID} provides information on the amount of cumulated gas, as the CID triggering and vent activation pressure are independent of the cell state. Therefore, it can be concluded that the amount of gas increases linearly with SOC, which is consistent with the findings of Jindal et al.[4] and Chen et al.[21] This can be explained by the fact of a higher intercalated Li content in the anode with increasing SOC, causing more gas production due to the decomposition and reformation of the SEI.[20,73] Ishikawa et al. confirmed the increased gas production with increasing SOC through storage tests at 100 °C and observed minor gas production in fairly stable electrodes at 0 % SOC.[25]

All aged cells, except those aged at RT with 100% SOC, exhibit a lower T_{CID} than new cells. Within the scattering of the data in Figs. 5c and 5d, there is a slight trend of a lower T_{CID} for 0 °C and 50 °C aged cells compared to RT aged cells. This could be due to additional gas formation possibly already during the aging process or an increase in gas generation during the ARC test, leading to a faster reaching of the critical CID triggering pressure. In general, and especially in combination with Li plating, the electrolyte composition has a significant influence on the amount of gas produced.[74] In particular the aged cells with reduced energy content show that the SOC has a greater influence than the energy content on T_{CID}.

The venting temperature (see Figs. 5e and 5f) follows a similar trend as T_{CID}, with an average temperature that is 9 K higher at increased scattering. 0 °C aged cells at 100% SOC particularity show the lowest CID triggering and venting temperature. This might be due to much longer test durations, which allow the components to react longer under more gas formation. This is a consequence of the low T_{SH} in combination with very low SHR below approximately 100 °C.

The TR onset temperature (T_{TR}) exhibits a decreasing trend with increasing SOC for all cells, as shown in Figs. 5g and 5h. This trend is consistent with the onset temperatures observed in literature for NMC cells above approximately 200 °C.[8,9,15,25–27] The TR is triggered by the decomposition of the cathode under oxygen release (see below), which further reacts with the electrolyte. Therefore, T_{TR} is directly related to the thermal stability of the cathode. A high SOC is associated with a higher degree of de-lithiation of the cathode. This leads to a destabilization of the NMC structure, which is in turn associated with a reduced thermal stability and a lower T_{TR}.[20,22]

The SOC dependence of T_{TR} is similar for new and aged cells. However, it is shifted towards lower temperatures, indicating a decrease in thermal stability of the aged Ni-rich cathode. This is consistent with the aging effects of the NMC cathode active material shown in Fig. 1b. Jindal et al. reported a significant degradation of the NMC material, resulting in a very low thermal stability.[4] In contrast to that, Friesen et al.,[20] Börner et al.,[22] and Feinauer et al.[17] observed only minor changes in the onset of TR temperature for graphite||NMC532 and graphite||NCA-LCO cells, indicating that the cathode stability remained unchanged during aging. Furthermore, it appears that both dominant aging mechanisms on the anode side, namely Li plating at low temperatures and accelerated SEI growth at high temperatures, have an impact on the stability of the cathode as observed by a slightly reduced T_{TR}. Figure 5h shows an even more distinct degradation of the thermal stability with aging as a function of the stored electrical energy. This indicates that the SOC and aging state of the cell have the greater impact on the thermal stability of the cathode than the energy content.

T_{TR} is further correlated with the maximum SHR (see Fig. 2) and maximum temperature (see Fig. S5), both of which increase with SOC. However, it needs to be noted that the measurement of the maximum temperature is highly prone to errors and the internal temperature could be significantly higher.[75] The intensity of TR can

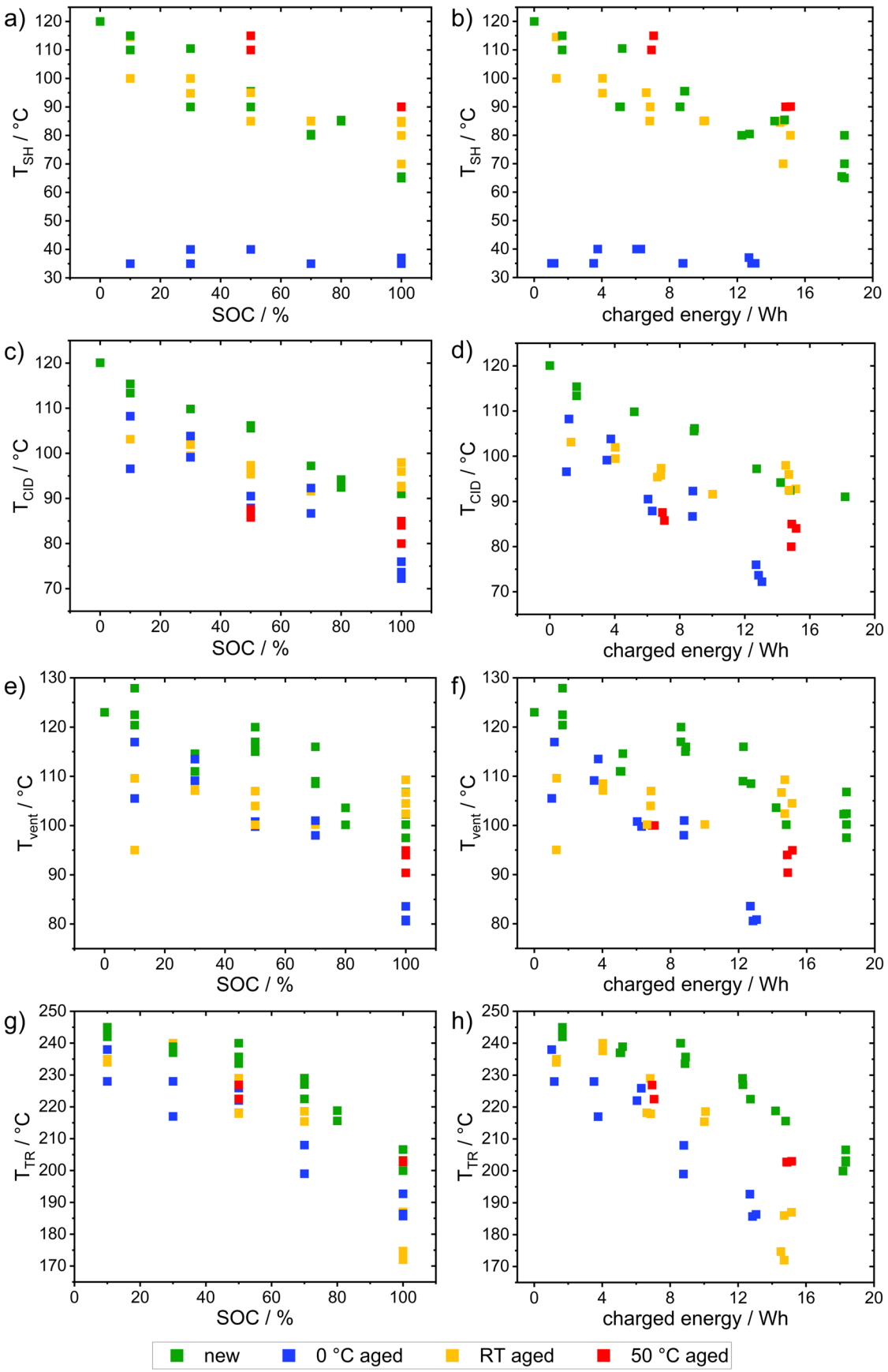

Figure 5. Characteristic temperatures as a function of SOC and charged energy for new cells and cells aged at different temperatures: (a), (b) the onset of SH, (c), (d) the CID triggering, (e), (f) the venting, and (g), (h) the onset of TR.

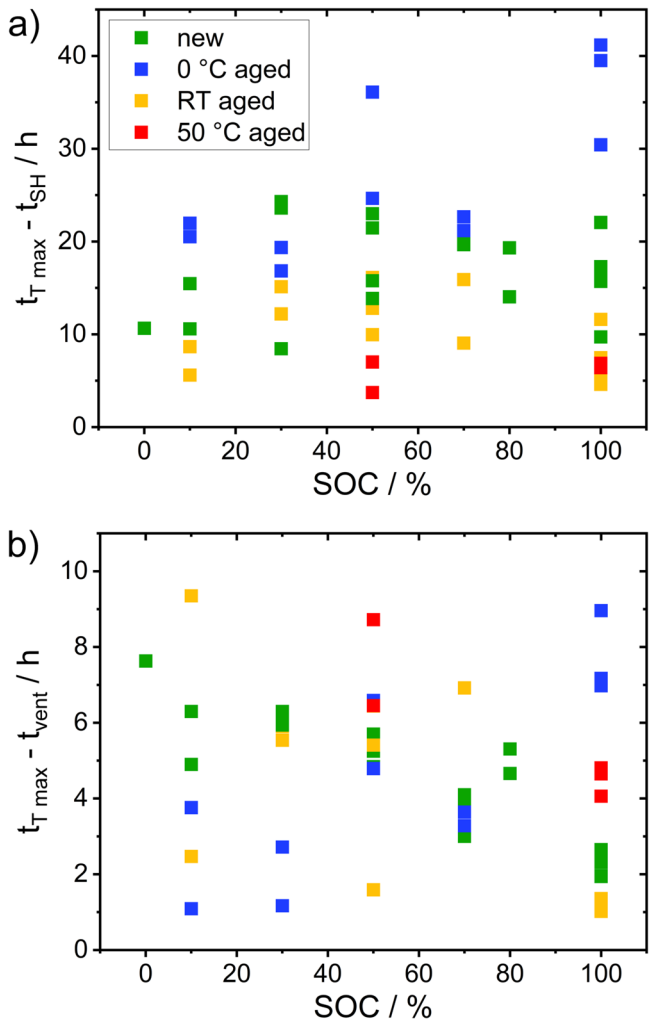

Figure 6. Time difference between (a) onset of SH and (b) venting and point of maximum temperature. The longer the time difference, the greater the likelihood of stopping the cell before TR.

also vary by orders of magnitude as a function of SOC.[8,19,25,28,32] Although the onset of TR is decreased for all aged cells, the maximum SHR and maximum temperature do not show significant changes. This is in contrast to various other safety tests of aged cells, showing reduced maximum temperatures for aged cells.[12,76]

Early detection of unsafe cells requires monitoring of not only critical temperatures but also of the time available to intervene. Thus, Figs. 6a and 6b display the time from the onset of SH and venting to the point of maximum temperature for all cells as a function of SOC, respectively. The onset of SH is defined as the first safety critical temperature, and the venting is considered as an easily detectable event.[17] The longer the time differences shown in Fig. 6, the greater the likelihood of preventing the TR.

No clear trend for the time difference between the onset of SH and point of maximum temperature during TR as a function of SOC can be observed in Fig. 6a. However, a tendency is visible for the different aging temperatures. The low onset of SH for the cells aged at 0 °C leads to a longer time until the onset of TR occurs. In contrast, the RT and, in particular, the 50 °C aged cells show a much shorter time between the onset of SH and point of maximum temperature due to the high T_{SH} but similar TR behavior. The new cells were intermediate between the high and low temperature aged cells.

The time between venting and maximum temperature decreases as the SOC increases for new cells (see Fig. 6b). This is consistent with Kim et al.[77] and exacerbates the safety issue of cells with increasing SOC. No SOC dependent trend for the time between venting and maximum temperature is visible in Fig. 6b for the RT and 50 °C aged cells. The cells with Li plating show the shortest times from venting to the point of maximum temperature at low SOCs.

Cell destruction and mass loss.—Cell destruction and mass loss are closely related because a heavily damaged cell usually results in a significant mass loss. These factors can also be linked to the intensity of TR and the amount of heat generated.

Figure 7 shows photographs of the new 21700 cells after ARC testing at different SOC. Aged cells, irrespective of their aging temperature, appear similar to fresh cells at medium SOC levels. However, in aged cells with 10% SOC, the jelly roll is ejected and the can is slightly damaged at the bottom (see Fig. S6). At 100% SOC in aged cells, the lid is opened (see Fig. S6). Additionally, two

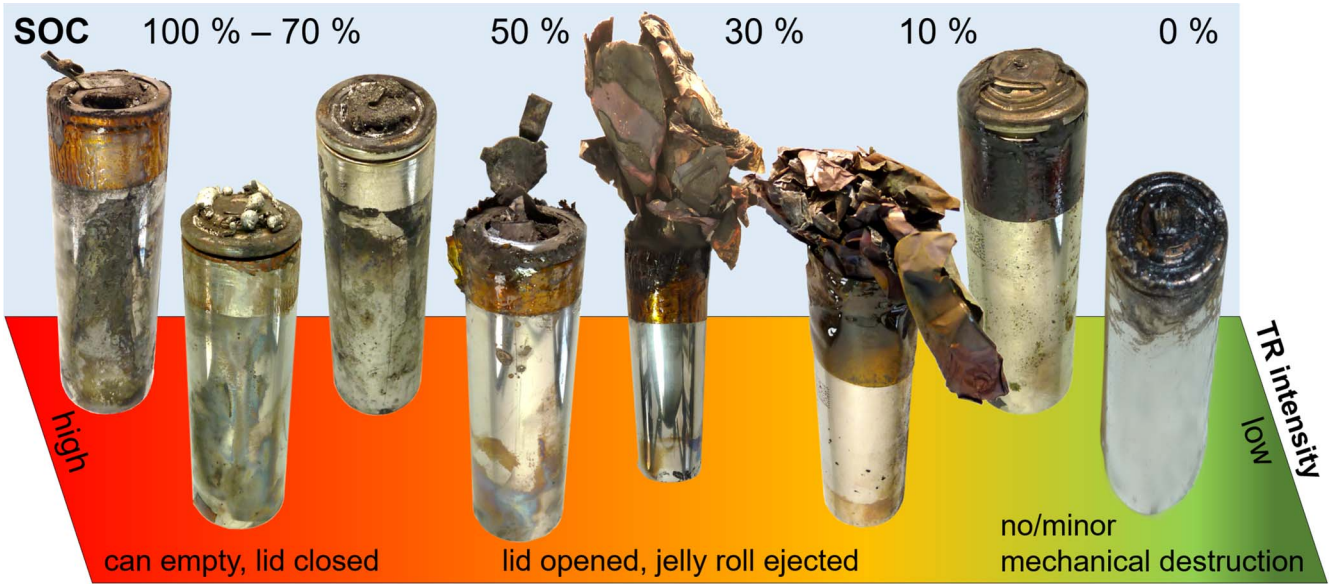

Figure 7. Photographs of new 21700 cells after ARC tests for different SOC. The level of destruction and thus TR intensity increase with SOC. At low SOC, no or only minor mechanical destruction is observed. At medium SOC, the lid opens and the jelly roll becomes ejected. At high SOC, the jelly roll becomes pulverized and the can is emptied through the top, even if the lid remains in position.

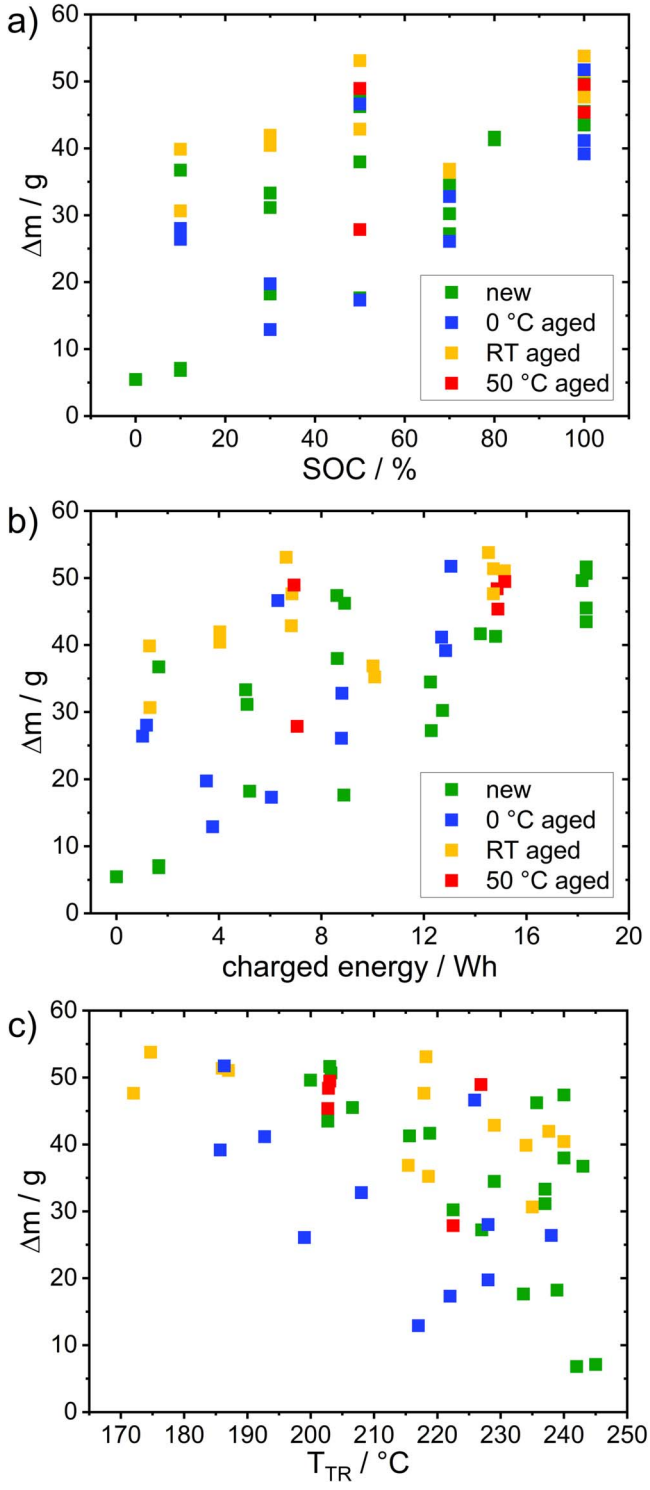

Figure 8. Mass loss of new and differently aged 21700 cells after ARC tests as a function of (a) SOC, (b) charged energy and (c) TR onset temperature.

cells with Li plating (100% and 70% SOC) showed a small melt hole in the bottom of the can (see Fig. S6). However, this was not reproducible for both cell states. In conclusion, aged cells tend to show a higher level of destruction in ARC tests. The higher destruction level in particular of cell with Li plating is consistent with other 18650 cells containing graphite||NMC-LMO and graphite||NCA tested at 100% SOC, where only aged cells with Li plating showed ejection of the jelly roll.[14,37]

Three levels of destruction based on SOC can be defined for the cells used in this publication. At low SOC ($\leqslant$10%), no or only minor destruction of the cell case is observed and the cell housing stays mostly intact. The classification by EUCAR[78] hazard level results in a hazard level of 3 to 4 out of 7. However, the situation changes significantly for cells in the medium SOC range (10% $<$ SOC $\leqslant$ 50 %). The lid was opened and the jelly roll was partially ejected and crumpled, indicating a strong internal pressure increase before ejection. Additionally, the destruction pattern shows many parts of the active mass distributed over the ARC-vessel. Therefore, this type of cell explosion must be associated with higher EUCAR[78] levels of 6–7.

Upon initial inspection, cells with a high SOC (>50%) appear to be less damaged than those with medium SOC. However, even if the cell still appears intact from the outside and even if the lid is still closed, the can is empty. This indicates that the entire jelly roll must have decomposed and must have been ejected in a pulverized form through the venting holes of the lid. The pulverization of the jelly roll is in good agreement with the increased particle density in the gas emitted during a battery fire at high SOC, as detected by Kim et al.[77] There is no consensus on the critical SOC above which violent flames and fire was observed, as different authors report different values depending on the cell type.[7] Chen et al.[79] reported an SOC of 50%, while He et al.[80] observed flames only for SOC $>$ 80%. Nguyen et al.[29] attributed the ejection of the jelly roll at the medium SOC to a delayed internal short circuit and a higher T_{vent} compared to cells with high SOC, resulting in stronger exothermic reactions at this time. This is also consistent with Ohneseit et al., who found the highest degree of destruction at 30% SOC.[8]

Regardless of the cell's SOC, the photographs in Fig. 7 demonstrate that the cell's safety design is effective, as venting occurs at the top only. This information is crucial for designing safety measures in battery systems. However, a small hole was burned into the bottom of some cells at high SOC.

Figure 8 displays the mass loss Δm of the cells after the ARC testing. It should be noted that measuring the mass accurately can be challenging and prone to errors, especially if the jelly roll is only partly ejected. A new cell weighs about 68.9 g in total, including a weight of 11.7 g for can and lid. Since the can remained intact throughout all tests, the mass loss is limited to about 57 g.

Furthermore, Figs. 8a and 8b show the expected relation that a high SOC and energy content are correlated to a high mass loss. However, low SOC and energy content do not necessarily lead to a low mass loss. No discernible trend is evident when comparing new and aged cells. The mass loss as a function of T_{TR} in Fig. 8c shows that a more harsh reaction of the cell, indicated by an earlier TR, results in a higher mass loss. The cells aged at 0 °C are distinguishable from the others due to their lower mass losses at a certain T_{TR}. This is because the ejected jelly roll remains partially in the cell can and is therefore not taken into account in the mass loss.

In conclusion, the results presented in Figs. 7 and 8 demonstrate that cell reactivity and mass loss increase with SOC and energy content in both new and aged cells, which is consistent with literature.[4,29,77,81] Chen et al.[21] also found that the explosion energy of an 18650 cell increases from 1.1 kJ to 8.7 kJ as the SOC increases from 30% to 100%. However, our data in context with literature show that the reaction strength during TR depends also on the main aging mechanism and cell type and has to be measured for each cell type and cell state.

Gas analytics.—Figures 9 and S7 represent the emitted gases during the thermal abuse test of new and aged cells at various SOC. The MS profiles show four characteristic regions of the recorded signals parallel to the four stages of the cell thermal behavior: (i) the zero-signal (baseline) before the first gas release from the cells, (ii) the small peak at the cell venting, followed by (iii) an almost constant gas formation due to ongoing decomposition reactions, and (iv) the highest signals at the TR of the cell.

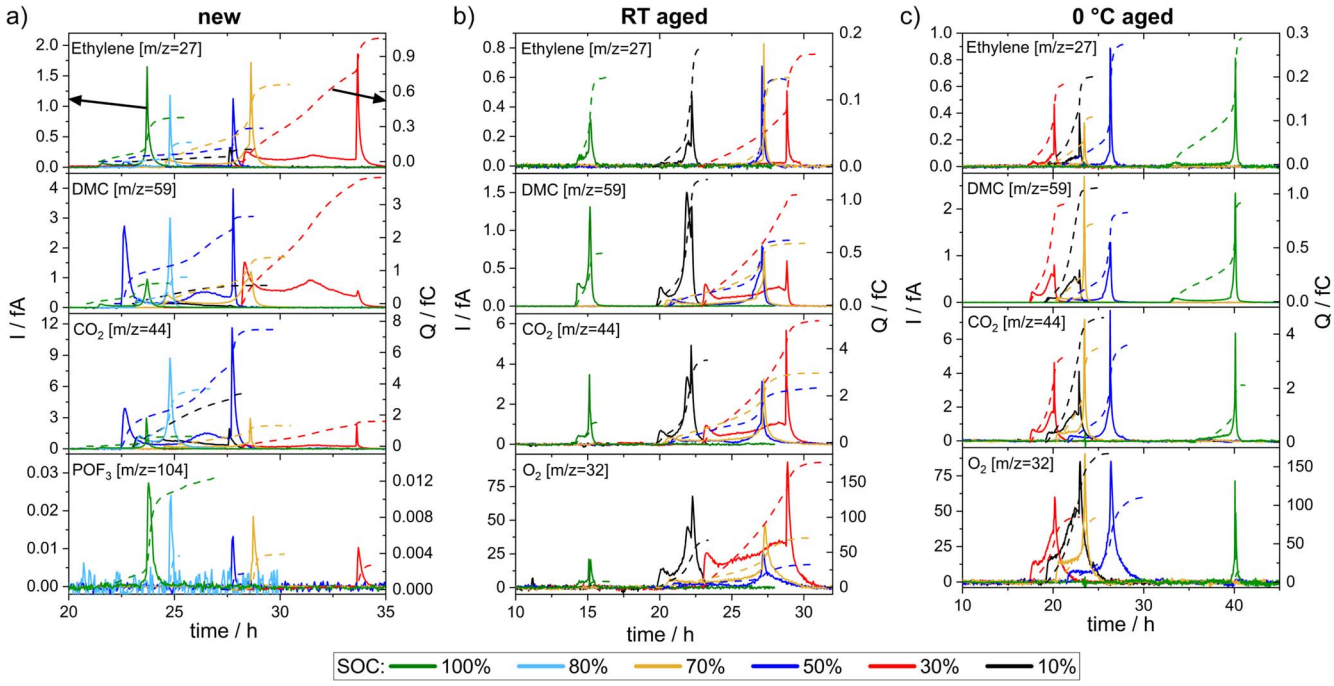

Figure 9. Mass spectrometric ionic current I (solid lines) and the integrated ionic charges Q (dashed lines) for $m/z = 44$ (CO_2), 27 (C_2H_4), 59 (DMC), 104 (POF_3), and 32 (O_2) during the ARC test of 21700 cells at various SOC for (a) new cells, (b) aged cells at RT, and (c) aged cells at 0 °C.

The prevailing component of the evolved gases during the cell venting of new and RT aged cells is the vapor of organic solvents (DMC) originating most likely from the electrolyte in addition to a minor signals of decomposition products such as C_2H_4, CO_2, and POF_3. The long time difference between venting and onset of TR of the cells at low SOC, due to the lower SHR, allows greater accumulation of the gases. Consequently, higher integrated signals are found compared to those produced at a high SOC, i.e. high reaction rates. This is similar to our earlier study with 18650 cells with graphite||NCA chemistry, where aged cells showed less gas evolution and shorter times until TR.[16] For a semi-quantitative analysis, the ionic charges have been integrated (dashed lines) as shown in Fig. 9. It is obvious from the integrated charges of the detected gases that the new cells produce more ethylene (C_2H_4) and vapor of DMC especially at low SOC than aged cells. Cells aged at RT show the highest CO_2 formation at 30% SOC, followed by the cells aged at 0 °C and the new cell.

Signals of O_2 were not detectable during the thermal abuse of new cells at high SOC (>50%). We attribute this to the amount of O_2 being out of the secondary electron multiplayer sensitivity limit. However, the thermal instability of the de-lithiated cathode in the presence of electrolyte results in oxygen evolution (Figs. 9b, 9c) and hence exothermic reactions.[82] Aged cells, either at RT or at 0 °C, show the evolution of O_2 resulting from the decomposition of cathode material,[83] combined with a recorded signal for $m/z = 2$ (the on-line MS could not distinguish between the overlapping signals of H_2 and fragments of organic species). The higher amount of oxygen released as shown Figs. 9b, 9c could help to understand the high destruction degree of the aged cells at low to medium SOC. Ohneseit et al. reported the emission of the explosive gases (H_2 and O_2 mixture) in the low SOC cells by GC-MS ex situ gas analysis of similar NMC 21700 cells.[8] TR experiments of 18650 NCA cells with various SOC showed an almost linear increase in the amount of gas,[84] in particular the amount of H_2 and CO increased while the amount of CO_2 decreased. It is obvious that the integrated ionic signals of the emitted gases in the aged cells are lower than those of the new cells, regardless of the SOC. We attribute this behavior to the reduced amount of reactive Li and less electrolyte in the aged cell, as previously reported by Essl et al.[36]

Conclusions

ARC-HWS tests were conducted on 48 new and aged 21700 cylindrical Li-ion battery cells at various SOC to determine their safety-critical temperatures. Simultaneous recording of the cell voltage until the CID activation provided important insights into the ongoing chemical and thermal processes during thermal abuse experiments. The produced gases were detected through an externally coupled online-MS.

The cells were subjected to cyclic aging until 80% SOH at 0 °C, RT, and 50 °C, each triggering different dominating aging mechanisms. Aging at 0 °C caused a rapid drop in capacity due to Li plating on the anode and subsequent LLI, while cycling at RT and 50 °C resulted in a capacity loss due to the loss of the Si component in the anode (LAAM) and LLI due to strong SEI growth. The DVA also indicated losses in cathode capacity for all aged cells (LCAM).

The results of the ARC HWS tests indicate clear trends for the critical temperatures and TR intensity as a function of aging and SOC. These trends are shown in Fig. 10 and can be summarized as follows:

- The onset of SH increases with decreasing SOC, similarly for new and RT aged cells. 50 °C aged cells show the same trend with an offset towards higher temperatures.
- 0 °C aged cells with Li plating exhibit significant safety concerns due to the constantly low onset of SH, independent of the cell's SOC. Lower SOC lead to higher SHR of cells at low temperatures at the beginning of the ARC tests due to possible re-intercalation of the plated Li.
- The temperature at which the CID is triggered and the venting temperature decrease with increasing SOC. An increased amount of gas in aged cells further decreases these temperatures compared to the new cells, following a similar SOC dependency.
- The onset temperature of TR decreases with increasing SOC. Aging of the cells results in a further decrease of the TR onset temperature due to a lowered thermal stability of the degraded cathode. However, the SOC dependent trend remains similar for aged cells.
- The severity of TR, mass loss, and degree of cell destruction after ARC testing increase for cells at higher SOC, and are slightly

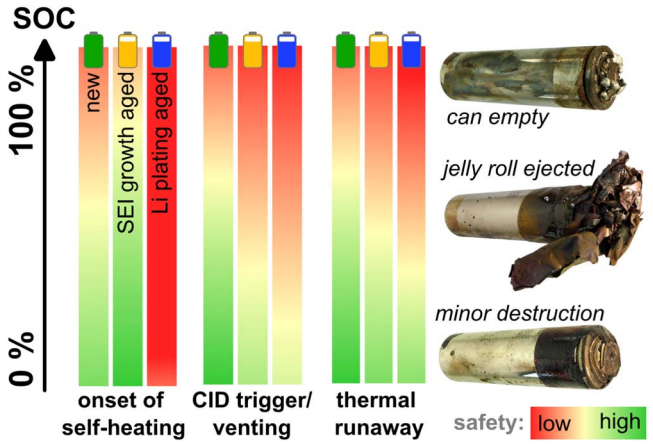

Figure 10. Summary of the ARC HWS safety test results for new and differently aged Ni-rich NMC 21700 cells at various SOC. Aged cells were distinguished by their dominant aging mechanism: Li plating and SEI growth after aging at low and high temperatures, respectively. The color of the bars indicates the safety as determined by the temperature of the critical events: onset of SH, CID trigger/venting, and onset of TR. Photographs of the cells after ARC testing at different SOC are shown.

higher for the aged cells. Notably, the jelly roll is only ejected as a whole in the medium SOC range. The lid remains closed at both low and high SOC levels. However, at high SOC, the can is emptied by pulverization of the jelly roll through the venting holes of the lid without destroying the lid. The safety devices of the cell were successfully triggered for almost all cells, which is a crucial knowledge when designing safety measures for battery systems. Only a few cells with Li plating exhibited an extra hole on the bottom of the cell can.

The benefit of a low onset of SH, particularly in cells with Li plating, is the increased time available to intervene before the irreversible TR occurs. The data obtained from the combined ARC-MS technique can be used to assess the safety implications of the reaction, identify potential reaction hazards, optimize reaction conditions, and develop mitigation strategies for industrial processes. It has to be noted that the ARC HWS tests give a first hint on the time to intervene and to stop a TR. However, in a real life scenario this still has to be evaluated for different triggers.

In conclusion, both aging and high SOC exhibit a diminished safety level for the investigated cell type in ARC HWS tests, particularly when both factors are present concurrently. Therefore, long-term storage and shipping of batteries is typically restricted to low SOC. With the exception of the onset of SH, the safety critical temperatures, such as venting or the onset of TR, are lower in aged cells, irrespective of the main aging mechanism. Furthermore, the extremely low onset of SH and the strong reactions during TR for aged cells with Li plating further emphasizes the critical need to prevent Li plating. We note that we have recently published workflows with validated methods for efficiently detecting and preventing Li plating which could be helpful here.[85]

To gain a more general view, in further work it will be important to consider the influence of the SOH alongside the SOC and different aging mechanisms for other cell types. Additionally, it will be beneficial to conduct different safety tests such as mechanical or electrical abuse tests. Further work into this direction is ongoing in our labs.

Acknowledgments

We gratefully acknowledge the German Federal Ministry of Education and Research (BMBF) for the financial support of the project AnaLiBa (03XP0347C) within the AQua cluster as well as the project management by the Projektträger Jülich (PtJ). We further thank M. Kasper (ZSW) and A. Aracil Regalado (ZSW) for the Post-mortem analyses and helpful discussions.

ORCID

Max Feinauer https://orcid.org/0000-0003-2483-8257
Abdelaziz A. Abd-El-Latif https://orcid.org/0000-0002-4763-9827
Margret Wohlfahrt-Mehrens https://orcid.org/0000-0002-5118-5215
Markus Hölzle https://orcid.org/0009-0004-8278-1089
Thomas Waldmann https://orcid.org/0000-0003-3761-1668

References

1. M. Flügel, K. Richter, M. Wohlfahrt-Mehrens, and T. Waldmann, *J. Electrochem. Soc.*, **169**, 50533 (2022).
2. L. Ma, M. Nie, J. Xia, and J. R. Dahn, *J. Power Sources*, **327**, 145 (2016).
3. H. Kim, S-M. Oh, B. Scrosati, and Y-K. Sun, *Advances in Battery Technologies for Electric Vehicles* (Elsevier, Amsterdam) 191 (2015).
4. P. Jindal and J. Bhattacharya, *J. Electrochem. Soc.*, **166**, A2165 (2019).
5. S-M. Bak, E. Hu, Y. Zhou, X. Yu, S. D. Senanayake, S-J. Cho, K-B. Kim, K. Y. Chung, X-Q. Yang, and K-W. Nam, *ACS Appl. Mater. Interfaces*, **6**, 22594 (2014).
6. H-J. Noh, S. Youn, C. S. Yoon, and Y-K. Sun, *J. Power Sources*, **233**, 121 (2013).
7. T. Joshi, S. Azam, C. Lopez, S. Kinyon, and J. Jeevarajan, *J. Electrochem. Soc.*, **167**, 140547 (2020).
8. S. Ohneseit, P. Finster, C. Floras, N. Lubenau, N. Uhlmann, H. J. Seifert, and C. Ziebert, *Batteries*, **9**, 237 (2023).
9. A. Perea, A. Paolella, J. Dubé, D. Champagne, A. Mauger, and K. Zaghib, *J. Power Sources*, **399**, 392 (2018).
10. J. Lamb, L. Torres-Castro, J. C. Hewson, R. C. Shurtz, and Y. Preger, *J. Electrochem. Soc.*, **168**, 60516 (2021).
11. I. Bloom, S. A. Jones, E. G. Polzin, V. S. Battaglia, G. L. Henriksen, C. G. Motloch, R. B. Wright, R. G. Jungst, H. L. Case, and D. H. Doughty, *J. Power Sources*, **111**, 152 (2002).
12. Y. Preger, L. Torres-Castro, T. Rauhala, and J. Jeevarajan, *J. Electrochem. Soc.*, **169**, 30507 (2022).
13. K. C. Abbott, J. E. Buston, J. Gill, S. L. Goddard, D. Howard, G. E. Howard, E. Read, and R. C. Williams, *Journal of Energy Storage*, **65**, 107293 (2023).
14. T. Waldmann and M. Wohlfahrt-Mehrens, *Electrochim. Acta*, **230**, 454 (2017).
15. T. Waldmann, J. B. Quinn, K. Richter, M. Kasper, A. Tost, A. Klein, and M. Wohlfahrt-Mehrens, *J. Electrochem. Soc.*, **164**, A3154 (2017).
16. A. A. Abd-El-Latif, P. Sichler, M. Kasper, T. Waldmann, and M. Wohlfahrt-Mehrens, *Batteries & Supercaps*, **4**, 1135 (2021).
17. M. Feinauer, A. A. Abd-El-Latif, P. Sichler, A. Aracil Regalado, M. Wohlfahrt-Mehrens, and T. Waldmann, *J. Power Sources*, **570**, 233046 (2023).
18. D. Ouyang, M. Chen, J. Weng, K. Wang, J. Wang, and Z. Wang, *J. Energy Chem.*, **81**, 543 (2023).
19. H. M. Barkholtz, Y. Preger, S. Ivanov, J. Langendorf, L. Torres-Castro, J. Lamb, B. Chalamala, and S. R. Ferreira, *J. Power Sources*, **435**, 226777 (2019).
20. A. Friesen, F. Horsthemke, X. Mönnighoff, G. Brunklaus, R. Krafft, M. Börner, T. Risthaus, M. Winter, and F. M. Schappacher, *J. Power Sources*, **334**, 1 (2016).
21. W-C. Chen, Y-W. Wang, and C-M. Shu, *J. Power Sources*, **318**, 200 (2016).
22. M. Börner, A. Friesen, M. Grützke, Y. P. Stenzel, G. Brunklaus, J. Haetge, S. Nowak, F. M. Schappacher, and M. Winter, *J. Power Sources*, **342**, 382 (2017).
23. W. Li, K. R. Crompton, C. Hacker, and J. K. Ostanek, *J. Energy Storage*, **32**, 101890 (2020).
24. C. Mikolajczak, *Lithium-Ion Batteries Hazard and Use Assessment* (Springer New York, New York, NY) (2011).
25. H. Ishikawa, O. Mendoza, Y. Sone, and M. Umeda, *J. Power Sources*, **198**, 236 (2012).
26. N. E. Galushkin, N. N. Yazvinskaya, and D. N. Galushkin, *J. Electrochem. Soc.*, **165**, A1303 (2018).
27. E. Roth and D. Doughty, *J. Power Sources*, **128**, 308 (2004).
28. D. H. Doughty and E. P. Roth, *Electrochem. Soc. Interface*, **21**, 37 (2012).
29. T. T. D. Nguyen, S. Abada, A. Lecocq, J. Bernard, M. Petit, G. Marlair, S. Grugeon, and S. Laruelle, *World Electr. Veh. J*, **10**, 79 (2019).
30. A. Karmakar, H. Zhou, B. S. Vishnugopi, J. A. Jeevarajan, and P. P. Mukherjee, *J. Electrochem. Soc.*, **171**, 10529 (2024).
31. D. Ouyang, K. Wang, T. Gao, and Z. Wang, *J. Loss Prev. Process Ind.*, **80**, 104924 (2022).
32. C. Zhao, J. Sun, and Q. Wang, *J. Energy Storage*, **28**, 101232 (2020).
33. S. Abada, M. Petit, A. Lecocq, G. Marlair, V. Sauvant-Moynot, and F. Huet, *J. Power Sources*, **399**, 264 (2018).
34. F. Baakes, D. Witt, and U. Krewer, *Chem. Sci.*, **14**, 13783 (2023).
35. D. Ren et al., *eTransportation*, **2**, 100034 (2019).
36. C. Essl, A. W. Golubkov, and A. Fuchs, *Batteries*, **7**, 23 (2021).
37. M. Fleischhammer, T. Waldmann, G. Bisle, B-I. Hogg, and M. Wohlfahrt-Mehrens, *J. Power Sources*, **274**, 432 (2015).
38. Y. Li, X. Feng, D. Ren, M. Ouyang, L. Lu, and X. Han, *ACS Appl. Mater. Interfaces*, **11**, 46839 (2019).
39. T. Waldmann, M. Wilka, M. Kasper, M. Fleischhammer, and M. Wohlfahrt-Mehrens, *J. Power Sources*, **262**, 129 (2014).

40. T. Waldmann, B-I. Hogg, and M. Wohlfahrt-Mehrens, *J. Power Sources*, **384**, 107 (2018).
41. H. Baltruschat and A. A. Abd-El-Latif, *Encyclopedia of Applied Electrochemistry*, ed. G. Kreysa et al. (Springer New York, New York, NY) 507 (2014).
42. T. He, T. Zhang, S. Gadkari, Z. Wang, N. Mao, and Q. Cai, *J. Clean. Prod.*, **388**, 135980 (2023).
43. T. Gao, J. Bai, D. Ouyang, Z. Wang, W. Bai, N. Mao, and Y. Zhu, *Renew. Energy*, **203**, 592 (2023).
44. S. Xie, L. Ren, X. Yang, H. Wang, Q. Sun, X. Chen, and Y. He, *J. Power Sources*, **448**, 227425 (2020).
45. J. Zhang, L. Su, Z. Li, Y. Sun, and N. Wu, *Batteries*, **2**, 12 (2016).
46. G. Kucinskis, M. Bozorgchenani, M. Feinauer, M. Kasper, M. Wohlfahrt-Mehrens, and T. Waldmann, *J. Power Sources*, **549**, 232129 (2022).
47. X-G. Yang and C-Y. Wang, *J. Power Sources*, **402**, 489 (2018).
48. M. Bozorgchenani, G. Kucinskis, M. Wohlfahrt-Mehrens, and T. Waldmann, *J. Electrochem. Soc.*, **169**, 30509 (2022).
49. B. Y. Liaw, E. Roth, R. G. Jungst, G. Nagasubramanian, H. L. Case, and D. H. Doughty, *J. Power Sources*, **119-121**, 874 (2003).
50. S. Käbitz, J. B. Gerschler, M. Ecker, Y. Yurdagel, B. Emmermacher, D. André, T. Mitsch, and D. U. Sauer, *J. Power Sources*, **239**, 572 (2013).
51. I. Zilberman, J. Sturm, and A. Jossen, *J. Power Sources*, **425**, 217 (2019).
52. C. R. Birkl, M. R. Roberts, E. McTurk, P. G. Bruce, and D. A. Howey, *J. Power Sources*, **341**, 373 (2017).
53. C. Hogrefe, T. Waldmann, M. B. Molinero, L. Wildner, P. Axmann, and M. Wohlfahrt-Mehrens, *J. Electrochem. Soc.*, **169**, 50519 (2022).
54. P. Keil and A. Jossen, *J. Electrochem. Soc.*, **164**, A6066 (2017).
55. H. Park, T. Yoon, Y. Kim, J. G. Lee, J. Kim, H. Kim, J. H. Ryu, J. J. Kim, and S. M. Oh, *J. Electrochem. Soc.*, **162**, A892 (2015).
56. H. Yang, H. Bang, K. Amine, and J. Prakash, *J. Electrochem. Soc.*, **152**, A73 (2005).
57. K. M. Abraham, *J. Electrochem. Soc.*, **170**, 110508 (2023).
58. C. Misiewicz, R. Lundström, I. Ahmed, M. J. Lacey, W. R. Brant, and E. J. Berg, *J. Power Sources*, **554**, 232318 (2023).
59. A. W. Golubkov, D. Fuchs, J. Wagner, H. Wiltsche, C. Stangl, G. Fauler, G. Voitic, A. Thaler, and V. Hacker, *RSC Adv.*, **4**, 3633 (2014).
60. F. Larsson, S. Bertilsson, M. Furlani, I. Albinsson, and B-E. Mellander, *J. Power Sources*, **373**, 220 (2018).
61. X. Feng, M. Ouyang, X. Liu, L. Lu, Y. Xia, and X. He, *Energy Storage Mater.*, **10**, 246 (2018).
62. M. Feinauer, N. Uhlmann, C. Ziebert, and T. Blank, *Batteries*, **8**, 177 (2022).
63. G. L. Plett, *Battery Management Systems, Volume 1: Battery Modeling* (Artech House, Boston, London) (2015).
64. L. E. Downie, L. J. Krause, J. C. Burns, L. D. Jensen, V. L. Chevrier, and J. R. Dahn, *J. Electrochem. Soc.*, **160**, A588 (2013).
65. O. Y. Egorkina and A. M. Skundin, *J. Solid State Electrochem.*, **2**, 216 (1998).
66. C. Uhlmann, J. Illig, M. Ender, R. Schuster, and E. Ivers-Tiffée, *J. Power Sources*, **279**, 428 (2015).
67. C. Hogrefe, S. Hein, T. Waldmann, T. Danner, K. Richter, A. Latz, and M. Wohlfahrt-Mehrens, *J. Electrochem. Soc.*, **167**, 140546 (2020).
68. K. Richter, T. Waldmann, N. Paul, N. Jobst, R-G. Scurtu, M. Hofmann, R. Gilles, and M. Wohlfahrt-Mehrens, *ChemSusChem*, **13**, 529 (2020).
69. V. Zinth, C. von Lüders, M. Hofmann, J. Hattendorff, I. Buchberger, S. Erhard, J. Rebelo-Kornmeier, A. Jossen, and R. Gilles, *J. Power Sources*, **271**, 152 (2014).
70. C. von Lüders, V. Zinth, S. V. Erhard, P. J. Osswald, M. Hofmann, R. Gilles, and A. Jossen, *J. Power Sources*, **342**, 17 (2017).
71. T. Lian, P. J. S. Vie, M. Gilljam, and S. Forseth, *ECS Trans.*, **89**, 73 (2019).
72. H. Zhou, C. Fear, R. E. Carter, C. T. Love, and P. P. Mukherjee, *Energy Storage Mater.*, **66**, 103214 (2024).
73. X. Tang, G. Zhang, X. Wang, G. Wei, G. Han, J. Zhu, X. Wei, and H. Dai, *iScience*, **24**, 103088 (2021).
74. Q. Q. Liu, D. J. Xiong, R. Petibon, C. Y. Du, and J. R. Dahn, *J. Electrochem. Soc.*, **163**, A3010 (2016).
75. M. Feinauer, M. Hölzle, and T. Waldmann, *Electrochem. Soc. Interface*, **33**, 51 (2024).
76. Y. Jia, X. Gao, L. Ma, and J. Xu, *Adv. Energy Mater.*, **13**, 2300368 (2023).
77. S. W. Kim, S. G. Park, and E. J. Lee, *J. Loss Prev. Process Ind.*, **80**, 104851 (2022).
78. EUCAR, Battery requirements for future automotive applications: EG BEV&FCEV (2019).
79. H. Li, H. Chen, G. Zhong, Y. Wang, and Q. Wang, *J. Loss Prev. Process Ind.*, **61**, 122 (2019).
80. X. He, Z. Hu, F. Restuccia, J. Fang, and G. Rein, *Appl. Therm. Eng.*, **212**, 118621 (2022).
81. Z. Han, L. Zhao, J. Zhao, G. Xu, H. Liu, and M. Chen, *Fire*, **7**, 119 (2024).
82. J. R. Dahn, E. W. Fuller, M. Obrovac, and U. Von Sacken, *Solid State Ion.*, **69**, 265 (1994).
83. H. Zhang, H. Liu, L. F. J. Piper, M. S. Whittingham, and G. Zhou, *Chem. Rev.*, **122**, 5641 (2022).
84. A. W. Golubkov, S. Scheikl, R. Planteu, G. Voitic, H. Wiltsche, C. Stangl, G. Fauler, A. Thaler, and V. Hacker, *RSC Adv.*, **5**, 57171 (2015).
85. T. Waldmann et al., *J. Electrochem. Soc.*, **171**, 70526 (2024).